Prepared for submission to SPSC

NA64 Status Report 2019

The NA64 Collaboration[1]

Abstract:
The status of the NA64 experiment aiming at a search for a sub-GeV vector mediator (A') of dark matter (χ) production is presented. New results from the analysis of the combined 2016-2018 data sample on the $A' \to \chi\chi$ decay search are reported. The preliminary results on the search for the visible A' decays $A' \to e^+e^-$ and $X \to e^+e^-$ decays of a 16.7 MeV X boson, which could explain an excess of e^+e^- pairs from the excited ^{8}Be nucleus transitions, are also presented. Ongoing activities on the detector preparation for the 2021 run are reviewed.

CERN-SPSC-2019-024 / SPSC-SR-255
07/06/2019

[1] http://na64.web.cern.ch/

Contents

1 Introduction

In a class of well motivated dark matter models, a new force between the dark sector and visible matter transmitted by a new vector boson A' (dark photon) might exist, see e.g. [1–4]. Such A' could have a mass $m_{A'} \lesssim 1$ GeV - associated with a spontaneously broken gauged $U(1)_D$ symmetry- and couple to the standard model (SM) through kinetic mixing with the ordinary photon, $-\frac{1}{2}\epsilon F_{\mu\nu}A'^{\mu\nu}$, parametrized by the mixing strength $\epsilon \ll 1$. If the A' is the lightest state in the dark sector, then it would decay mainly visibly, i.e., typically to SM leptons $l = e, \mu$ or hadrons, which could be used to detect it. However, in the presence of light dark states, in particular dark matter, with the masses $\lesssim 0.5 m_{A'}$, the A' would predominantly decay invisibly into those particles provided that their dark coupling constant $e_D > \epsilon e$.

The NA64 collaboration currently focuses on searches for the $A' \to invisible$ decay and other rare processes with the H4 electron beam with the main goal to accumulate in total up to $\gtrsim 5 \times 10^{12}$ electrons on target (EOT) in order to probe most of the remaining $(\epsilon; m_{A'})$ parameter space and unexplored parameter regions of sub-GeV dark matter models. In the following sections, we briefly summarize the performance of the detector during the 2018 run, and give the current status of the data analysis and obtained results.

2 The detector and ongoing activities

The NA64 detector is schematically shown in Fig. 1. The experiment employed the optimized H4 100 GeV electron beam. The beam has a maximal intensity $\simeq 10^7$ per SPS spill of 4.8 s produced by the primary 400 GeV proton beam with an intensity of few 10^{12} protons on target. The detector utilized the beam defining scintillator (Sc) counters S_{1-4} and veto $\mathrm{V}_{1,2}$, magnetic spectrometer consisting of two successive dipole magnets $\mathrm{MBPL}_{1,2}$ with the integral magnetic field of $\simeq$7 T·m and a low-material-budget tracker. The tracker was a set of two upstream Micromegas chambers $\mathrm{MM}_{1,2}$, and four MM_{3-6}, downstream stations, as well as two straw-tube $\mathrm{ST}_{1,2}$ and $\mathrm{GEM}_{1,2}$ chambers allowing the measurements of e^- momenta with the precision $\delta p/p \simeq 1\%$ [5]. To enhance the electron identification their synchrotron radiation (SR) emitted in the MBPL magnetic field was used for their efficient tagging with a SR detector (SRD), which was an array of PbSc sandwich calorimeter of a very fine segmentation [6, 7]. By using the SRD the initial admixture of the hadron contamination in the beam $\pi/e^- \lesssim 10^{-2}$ was further suppressed by a factor $\simeq 10^3$. The detector was also equipped with an active dump target, which is an electromagnetic calorimeter (ECAL), a matrix of 6×6 Shashlik-type modules assembled from Pb and Sc plates for measurement of the electron energy E_{ECAL}. Each module was $\simeq 40$ radiation lengths (X_0) with the first $4X_0$ served as a pre-shower detector. Downstream the ECAL the detector was equipped with a large high-efficiency veto counter (VETO),

and a massive, hermetic hadronic calorimeter (HCAL) of $\simeq 30$ nuclear interaction lengths in total. The modules HCAL_{1-3} served as an efficient veto to detect muons or hadronic secondaries produced in the $e^- A$ interactions in the target, while the zero-degree calorimeter HCAL_0 was used to reject events accompanied by a hard neutrals from the upstream e^- interactions. The new straw-tube tracker is manufactured with

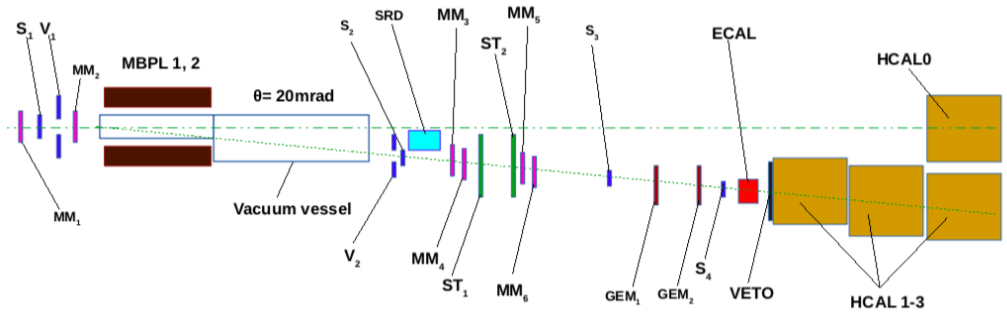

Figure 1. Schematic illustration of the setup to search for $A' \to \textit{invisible}$ decays of the bremsstrahlung A's produced in the reaction $eZ \to eZA'$ of 100 GeV e^- incident on the active ECAL target.

6 mm in diameter straw tubes covered by Cu layer. Each coordinate plane consist of two layers of straw shifted each other to the size of the radius. Two mother board for different layers are currently used. New 6 Amplifier AST-1-1 (32channels) for each coordinate which has to operate with 3 TDC units, are located directly on the each chamber stand. Cables are 17 twisted pairs, each of 60 cm in length. Since the 2017 run, the reconstruction of events in the straw tube tracker has been significantly improved.

2.1 Data sample from 2016-2018 runs

The events were collected with the hardware trigger requiring an in-time cluster in the ECAL with the energy $E_{ECAL} \lesssim 80 - 85$ GeV. The results reported here came mostly from a set of data in which $n_{EOT} = 4.3 \times 10^{10}$ of electrons on target (EOT) were collected with the beam intensity ranging from $\simeq 1.5 \times 10^6$/spill to $\simeq 5 \times 10^6$/spill e^- per spill in the year 2016, about $n_{EOT} = 5.4 \times 10^{10}$ collected with intensity $\simeq (5-6) \times 10^6$ e^-/spill in the year 2017, and $n_{EOT} = 1.87 \times 10^{11}$ collected with intensity up to $\simeq (8-9) \times 10^6$ e^-/spill in the year 2018. The total statistics thus corresponds to $n_{EOT} = 2.84 \times 10^{11}$ EOT. Data of these three runs were analyzed with similar selection criteria and finally summed up, taking into account the corresponding normalization factors. The combined analysis is described below.

3 Search for the $A' \to invisible$ decay

The idea is that a new, additional to gravity force between the dark and visible matter transmitted by a vector boson, A' , called dark photon, might exist, see e.g. [2]. The A' can have a mass in the sub-GeV mass range, and couple to the standard model (SM) via kinetic mixing with the ordinary photon, described by the term $\frac{\epsilon}{2}F'_{\mu\nu}F^{\mu\nu}$ and parameterized by the mixing strength ϵ. An example of the Lagrangian of the SM extended by the dark sector (DS) is given by:

$$\mathcal{L} = \mathcal{L}_{SM} - \frac{1}{4}F'_{\mu\nu}F'^{\mu\nu} + \frac{\epsilon}{2}F'_{\mu\nu}F^{\mu\nu} + \frac{m^2_{A'}}{2}A'_{\mu}A'^{\mu} + i\bar{\chi}\gamma^{\mu}\partial_{\mu}\chi - m_{\chi}\bar{\chi}\chi - e_D\bar{\chi}\gamma^{\mu}A'_{\mu}\chi, \tag{3.1}$$

where the massive A'_{μ} field is associated with the spontaneously broken $U_D(1)$ gauge group, $F'_{\mu\nu} = \partial_{\mu}A'_{\nu} - \partial_{\nu}A'_{\mu}$, e_D is the coupling strength of the $U(1)_D$ gauge interactions, and $m_{A'}$, m_{χ} are, respectively, the masses of the A' and dark matter (DM) particles, χ, which are treated as Dirac fermions coupled to A'_{μ} with the dark coupling strength e_D. The mixing term of (3.1) results in the interaction $\mathcal{L}_{int} = \epsilon e A'_{\mu}J^{\mu}_{em}$ of dark photons with the electromagnetic current J^{μ}_{em} with a strength ϵe, where e is the electromagnetic coupling and $\epsilon \ll 1$. Such small values of ϵ can be obtained in GUT from loop effects of particles charged under both the dark $U_D(1)$ and SM $U(1)$ interactions with a typical 1-loop value $\epsilon = ee_D/16\pi^2 \simeq 10^{-2} - 10^{-4}$, or from 2-loop contributions resulting in $\epsilon \simeq 10^{-3} - 10^{-5}$. The accessibility of these values at accelerator experiments has motivated a worldwide effort towards dark forces and other portals between the visible and dark sectors, see Refs. [1–4] for a review.

If the A' is the lightest state in the dark sector, then it would decay mainly visibly to SM leptons l (or hadrons) [4]. In the presence of light DM states χ with the masses $m_{\chi} < m_{A'}/2$, the A' would predominantly decay invisibly into those particles provided that $e_D > \epsilon e$. Various dark sector models motivate the existence of sub-GeV scalar and Majorana or pseudo-Dirac DM coupled to the A'. To interpret the observed abundance of DM relic density, the requirement of the thermal freeze-out of DM annihilation into visible matter through $\gamma - A'$ mixing allows one to derive a relation

$$\alpha_D \simeq 0.02 f \left(\frac{10^{-3}}{\epsilon}\right)^2 \left(\frac{m_{A'}}{100\ MeV}\right)^4 \left(\frac{10\ MeV}{m_{\chi}}\right)^2 \tag{3.2}$$

where $\alpha_D = e^2_D/4\pi$, $f \lesssim 10$ for a scalar, and $f \lesssim 1$ for a fermion . This prediction provide an important target for the $(\epsilon,\ m_{A'})$ parameter space which can be probed at the CERN SPS energies. Models introducing the invisible A' also allow to explain various astrophysical anomalies and are subject to various experimental constraints leaving, however, a large area that is still unexplored.

Here, we report new results on the search for the A' mediator and light dark matter (LDM) in the fixed-target experiment NA64 at the CERN SPS. In the following we

assume that the A' invisible decay mode is predominant, i.e. $\Gamma(A' \to \bar{\chi}\chi)/\Gamma_{tot} \simeq 1$. If such invisible A' exists, many crucial questions about its coupling constants, mass scale, decay modes, etc. arise. One possible way to answer these questions, is to search for the A' in fixed-target experiments. The A's could be produced by a high intensity beam in a dump and generate a flux of DM particles through the $A' \to \bar{\chi}\chi$ decay, which can be detected through the scattering off electrons in the far target . The signal event rate in the detector in this case, scales as $\epsilon^2 y \propto \epsilon^4 \alpha_D$, with one ϵ^2 associated with the A' production in the dump and $\epsilon^2 \alpha_D$ coming from the χ particle scattering in the detector, and with the parameter y is defined as

$$y = \epsilon^2 \alpha_D \Big(\frac{m_\chi}{m_{A'}}\Big)^4. \tag{3.3}$$

Another method, proposed in Refs. [7, 8], is based on the detection of the missing energy, carried away by the energetic bremsstrahlung A' produced in the process $e^- Z \to e^- Z A'; A' \to invisible$ of high-energy electrons scattering in the active beam dump target. If the A' exists it could be produced via the kinetic mixing with bremsstrahlung photons in the reaction of high-energy electrons scattering off nuclei of an active target of a hermetic detector, followed by the prompt $A' \to invisible$ decay into dark matter particles (χ):

$$e^- Z \to e^- Z A'; A' \to invisible \tag{3.4}$$

A fraction f of the primary beam energy $E_{A'} = fE_0$ is carried away by χs which penetrate the detector without interactions resulting in an event with zero-energy deposition. While the remaining part $E_e = (1-f)E_0$ is deposited in the target by the scattered electron. Thus, the occurrence of A' produced in the reaction (4.1) would appear as an excess of events whose signature is a single electromagnetic (e-m) shower in the target with energy E_e accompanied by a significant missing energy $E_{miss} = E_{A'} = E_0 - E_e$ above those expected from backgrounds [7]. Here we assume that the χs have to traverse the detector without decaying visibly in order to give a missing energy signature. No other assumptions on the nature of the $A' \to invisible$ decay are made. The advantage of this type of experiment compared to the beam dump ones is that its sensitivity is proportional to ϵ^2, associated with the A' production and its subsequent prompt invisible decay,

3.1 Selection criteria and combined analysis

The results from the combined analysis of $n_{EOT} = 2.84 \times 10^{11}$ EOT collected during the years 2016-2018, hereafter are called respectively the run I,II,III. In order to avoid biases in the determination of selection criteria for signal events, a blind analysis was performed. Candidate events were requested to have the missing energy $E_{miss} > 50$ GeV. The signal box ($E_{ECAL} < 50\ GeV; E_{HCAL} < 1\ GeV$) was defined based on the calculations of the energy spectrum of A's emitted by $e^{\pm}$ from the e-m shower

generated by the primary e^-s in the target [9, 10]. A Geant4 based Monte Carlo (MC) simulation used to study the detector performance, signal acceptance, and background level, as well as the analysis procedure including selection of cuts and estimate of the sensitivity are described in detail in Ref.[11].

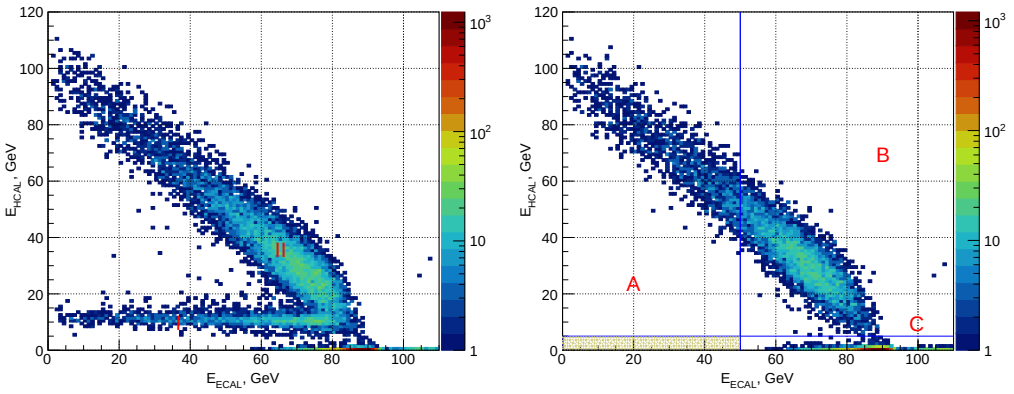

Figure 2. The left panel shows the measured distribution of events in the (E_{ECAL};E_{HCAL}) plane from the combined run data at the earlier phase of the analysis. Another panel shows the same distribution after applying all selection criteria. The dashed area is the signal box which is open. The size of the signal box along the E_{HCAL} axis is increased by a factor of 5 for illustration purposes. The side bands A and C are the ones used for the background estimate inside the signal region.

The left panel in Fig. 2 shows the distribution of $\simeq 3 \times 10^4$ events from the reaction $e^-Z \to anything$ in the $(E_{ECAL}; E_{HCAL})$ plane measured with loose selection criteria requiring mainly the presence of a beam e^- identified with the SR tag. Events from the area I in the left panel of Fig. 2 originate from the QED dimuon production, dominated by the reaction $e^-Z \to e^-Z\gamma; \gamma \to \mu^+\mu^-$ with a hard bremsstrahlung photon conversion on a target nucleus and characterized by the energy of $\simeq 10$ GeV deposited by the dimuon pair in the HCAL. This rare process was used as a benchmark allowing to verify the reliability of the MC simulation, correct the signal acceptance, cross-check systematic uncertainties and background estimate [11]. The region II shows the SM events from the hadron electroproduction in the target which satisfy the energy conservation $E_{ECAL} + E_{HCAL} \simeq 100$ GeV within the energy resolution of the detectors.

Finally, the following selection criteria were chosen to maximize the acceptance for signal events and to minimize the numbers of background events: (i) The incoming particle track should have the momentum 100 ± 3 GeV and a small angle with respect to the beam axis to reject large angle tracks from the upstream e^- interactions. (ii) The energy deposited in the SRD detector should be within the SR range emitted by e^-s and in time with the trigger. This was the key cut identifying the pure

initial e^- state. (iii) The lateral and longitudinal shape of the shower in the ECAL should be consistent with the one expected for the signal shower [9]. (iv) There should be no multiple hits activity in the Straw, which was an effective cut against hadron electroproduction in the beam material upstream the dump, and no activity in VETO. Only $\simeq 1.6 \times 10^4$ events passed these criteria from combined runs.

3.2 Background

The two largest sources of background which may fake the $A' \to invisible$ signal are expected from i) the mistakenly tagged beam μ, π, K decays in flight. For example, a particle passing through the vacuum vessel window could knock electrons off, which hit the SRD creating a fake tag for a e^-, and ii) the energy loss in events from nuclear e- interactions in the beam line due to the insufficient downstream detector coverage. The selection cuts to eliminate these backgrounds have been chosen such that they do not affect the shape of the true E_{miss} spectrum. Two complementary methods

Table 1. Expected background for 2.95×10^{11} EOT.

Background source	Background number, n_b
punchthrough γ's, cracks, holes	< 0.01
loss of dimuons	0.024 ± 0.007
$\mu \to e\nu\nu$, π, $K \to e\nu$, K_{e3} decays	0.02 ± 0.01
e^- interactions in the beam line	0.43 ± 0.16
μ, π, K interactions in the target	0.044 ± 0.014
accidental SR tag and μ, π, K decays	< 0.01
Total n_b	0.53 ± 0.17

based on the MC simulations and data themselves were used for the background estimation in the signal region. The relatively small event-number backgrounds such as the decays of the beam μ, π, K or μ from the reaction of dimuon production were simulated with the full statistics of the data. Large event-number processes from e^- interactions in the target or beam line, punchthrough of secondary hadrons were also studied extensively, although simulated samples with statistics similar to the data were not feasible. The background estimate in this case was mainly extracted from data by the extrapolation of events from sidebands A and C shown in the right panel of Fig. 2 into the signal region, assessing the systematic uncertainties by varying the background fit functions. We also examined the number of events observed in several regions around the signal box, which were statistically consistent with the estimates. Events in the region A ($E_{ECAL} < 50$ GeV; $E_{HCAL} > 1$ GeV) are pure neutral hadronic secondaries produced by electrons in the ECAL target, while events from the region C ($E_{ECAL} > 50$ GeV; $E_{HCAL} < 1$ GeV) are likely from the e^-

hadronic interactions in the downstream part of the beam line accompanied by the large transverse fluctuations of hadronic secondaries, which is difficult to simulate reliably. Table I summarizes the conservatively estimated background inside the signal region, which is expected to be 0.53 ± 0.17 events. After determining all the selection criteria and estimating background levels, we examined the events in the signal box and found no candidates, as shown in Fig. 2.

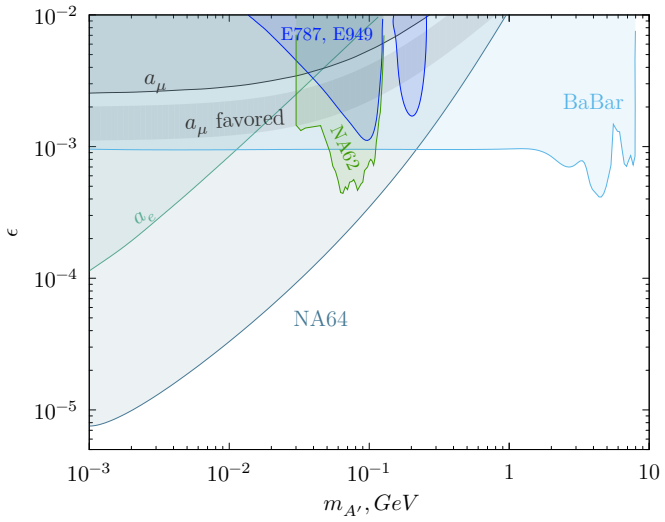

Figure 3. The NA64 90% C.L. exclusion region in the $(m_{A'}, \epsilon)$ plane. Constraints from the E787, E949 [1], BaBar [13] experiments, recent NA62 [14] results, as well as the muon α_μ favored area are also shown. Here, $\alpha_\mu = \frac{g_\mu - 2}{2}$. For more limits obtained from indirect searches and planned measurements see e.g. Ref. [1, 2].

3.3 Results and calculation of limits

This allows us to obtain the $m_{A'}$-dependent upper limits on the mixing ϵ which were calculated as follows. In the final combined statistical analysis the three runs I-III were analysed simultaneously using the multi-bin limit setting technique [11] based on the RooStats package [16]. First, the above obtained estimates of background, efficiencies, and their corrections and uncertainties were used to optimize better the main cut defining the signal box by comparing sensitivities, defined as an average expected limit calculated using the profile likelihood method. The calculations were done with uncertainties used as nuisance parameters, assuming their log-normal distributions [17]. For this optimization, the most important inputs were the expected values from the background extrapolation into the signal region from the data samples of the runs I,II,III. The errors for background prediction were estimated from the variation of the extrapolation functions. It was found that the optimal cut value depends very weakly on the A' mass choice and can be safely set to $E_{ECAL} < 50$ GeV for the whole mass range.

The combined 90% confidence level (C.L.) upper limits for ϵ were determined from the 90% C.L. upper limit for the expected number of signal events, $N_{A'}^{90\%}$ by using the modified frequentist approach for confidence levels (C.L.), taking the profile likelihood as a test statistic in the asymptotic approximation. The total number of expected signal events in the signal box was the sum of expected events from the three runs:

$$N_{A'} = \sum_{i=1}^{3} N_{A'}^{i} = \sum_{i=1}^{3} n_{EOT}^{i} \epsilon_{tot}^{i} n_{A'}^{i}(\epsilon, m_{A'}, \Delta E_e) \tag{3.5}$$

where ϵ_{tot}^{i} is the signal efficiency in the run i, and the $n_{A'}^{i}(\epsilon, m_{A'}, \Delta E_{A'})$ value is the signal yield per EOT generated in the energy range ΔE_e. Each i-th entry in this sum was calculated with simulations of signal events and processing them through the reconstruction program with the same selection criteria and efficiency corrections as for the data sample from the run-i. The expected backgrounds and estimated systematic errors were also taken into account in the limits calculation. The combined 90% C.L. exclusion limits on the mixing strength as a function of the A' mass can be seen in Fig. 3. The derived bounds are currently the best for the mass range $0.001 \lesssim m_{A'} \lesssim 0.1$ GeV obtained from direct searches of $A' \to$ *invisible* decays [4].

The overall signal efficiency, $\epsilon_{A'}$ is slightly $m_{A'}, E_{A'}$ dependent and is given by the product of efficiencies accounting for the geometrical acceptance (0.97), the tracker ($\simeq 0.83$), SRD ($\gtrsim 0.95$) veto VETO (0.94) and HCAL (0.94) signal efficiency, the acceptance loss due to pileup ($\simeq 8\%$) for high-intensity runs, and the DAQ dead time (0.93). The e^- beam loss due to interactions with the beam line materials was found to be small. The trigger (SRD) efficiency was found to be 0.95 (0.97) with a small uncertainty 2% (2%). The A' acceptance was evaluated by taking into account the selection efficiency for the lateral and longitudinal shape of e-m showers in the ECAL from signal events [9]. The A' production cross section in the primary reaction was obtained with the exact tree-level calculations as described in Refs.[10]. An additional uncertainty in the A' yield prediction $\simeq 10\%$ was conservatively accounted from the difference between the predicted and measured dimuon yield [11, 12]. The VETO and HCAL efficiency was defined as a fraction of events below the corresponding zero-energy thresholds. The spectrum of the energy distributions in these detectors from the leak of the signal shower energy in the ECAL was simulated for different A' masses [9] and cross-checked with measurements at the e^- beam. The uncertainty in the VETO and HCAL efficiency for the signal events, dominated mostly by the pileup effect from penetrating hadrons in the high intensity run III, was estimated to be $\lesssim 4\%$. Finally, the dominant source of systematic uncertainties on the expected number of signal events comes from the uncertainty in the estimate of the yield $n_{A'}(\epsilon, m_{A'}, \Delta E_{A'})$ (10%). The overall signal efficiency $\epsilon_{A'}$ for high-intensity runs varied from 0.65± 0.09 to 0.55±0.07 decreasing for the higher A' masses.

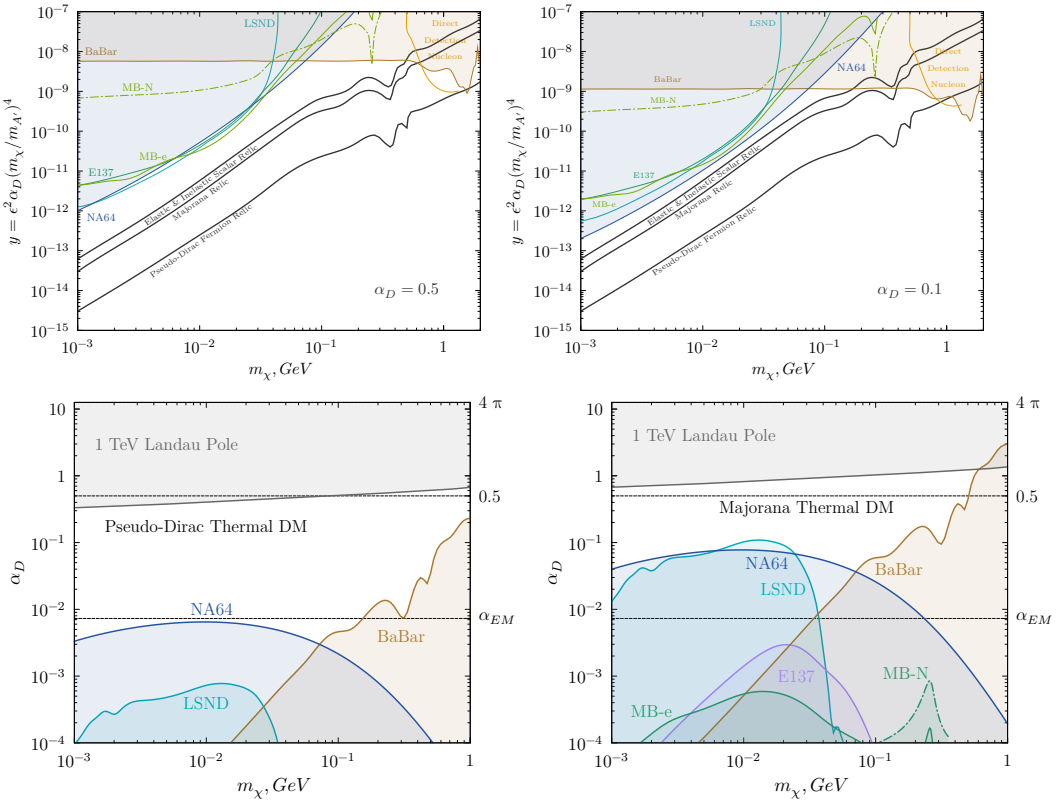

Figure 4. The top raw shows the NA64 limits in the (y;m_χ) plane obtained for $\alpha_D = 0.5$ (left panel) and $\alpha_D = 0.1$ (right panel) from the full 2016-18 data set. The bottom raw shows the NA64 constraints in the (α_D;$m_{A'}$) plane on the pseudo-Dirac (left panel) and Majorana (right panel) DM. The limits are shown in comparison with bounds from the results of the LSND and E137 [1], MiniBooNE [15], BaBar [13], and direct detection experiments . The favoured parameters to account for the observed relic DM density for the scalar, pseudo-Dirac and Majorana type of light DM are shown as the lowest solid line in top plots.

3.4 Constraints on sub-GeV dark matter

Using constraints on the cross section of the DM annihilation freeze out (resulting in Eq.(3.2)), and obtained limits on mixing strength of Fig. 3, one can derive constraints on the LDM models, which are shown in the (y;m_χ) and (α_D;m_χ) planes in Fig. 4 for the masses $m_\chi \lesssim 1$ GeV. The y limits are shown together with the favoured parameters for scalar, pseudo-Dirac (with a small splitting) and Majorana scenario of LDM taking into account the observed relic DM density [1]. The limits on the variable y are calculated by using Eq.(3.3) under the convention $\alpha_D = 0.1$ and =0.5, and $m_{A'} = 3m_\chi$ [1, 2]. This choice of the α_D region is compatible with the bounds derived based on the running of the dark gauge coupling arguments. The plot shows also the comparison of our results with bounds from other experiments. It should be noted that for smaller values of α_D NA64 limits will be stronger, due to the fact

that the signal rate in our case scales as ϵ^2, not as $\epsilon^4\alpha_D$ as for beam dump searches. The bounds on α_D for the case of pseudo-Dirac fermions shown in in Fig. 4 (left panel in the bottom raw) were calculated by taking the value $f = 0.25$ in Eq.(3.2) [11]. The limits for the Majorana case shown in the right panel in the bottom raw were calculated by setting $f = 3$ [11]. One can see that using the active beam dump approach allows us to obtain the most stringent bounds on ϵ, y, α_D for the mass range $m_\chi \lesssim 0.1$ GeV than the limits obtained from the results of classical beam dump experiments. This is mostly due to the fact that the experimental signature of $A' \to$ *invisible* decay events is clean and they can be identified with a small background due to the excellent capability of NA64 for the precise identification of the initial electron state.

4 Search for a new 16.7 MeV gauge boson from the ^{8}Be anomaly and dark photon decays $A' \to e^+e^-$

In this section we report the improved results on a direct search for a new 16.7 MeV boson (X) which could explain the anomalous excess of e^+e^- pairs observed in the excited ^{8}Be* nucleus decays. Due to its coupling to electrons, the X could be produced in the bremsstrahlung reaction $e^-Z \to e^-ZX$ by a beam of electrons incident on an active target in the NA64 experiment at the CERN SPS and observed through the subsequent decay into a e^+e^- pair. The data were collected in two runs of the experiment, in 2017 and 2018 corresponding in total to 8.4×10^{10} electrons on target.

The ATOMKI experiment of Krasznahorkay et al. [18] has reported the observation of a 6.8 σ excess of events in the invariant mass distributions of e^+e^- pairs produced in the nuclear transitions of excited $^8Be^*$ to its ground state via internal pair creation. It has been shown that the anomaly can be interpreted as the emission of a new protophobic gauge X boson with a mass of 16.7 MeV followed by its $X \to e^+e^-$ decay [19, 20]. This explanation of the anomaly was found to be consistent with all existing constraints assuming that the X has non-universal coupling to quarks, coupling to electrons in the range $2 \times 10^{-4} \lesssim \epsilon_e \lesssim 1.4 \times 10^{-3}$ and the lifetime $10^{-14} \lesssim \tau_X \lesssim 10^{-12}$ s. Interestingly, such relatively large charged lepton couplings can also resolve the so-called $(g_\mu - 2)$ anomaly, a discrepancy between measured and predicted values of the muon anomalous magnetic moment. This has motivated worldwide efforts towards the planned experimental searches, see, e.g. [21, 22], and various phenomenological aspects of light vector bosons weakly coupled to quarks and lepton, see e.g. [23]

Another strong motivation to the search for a new light boson decaying into e^+e^- pair is provided by the Dark Matter puzzle. An intriguing possibility is that in addition to gravity a new force between the dark sector and visible matter, transmitted

by a new vector boson, A' (dark photon), might exist . Such A' could have a mass $m_{A'} \lesssim 1$ GeV, associated with a spontaneously broken gauged $U(1)_D$ symmetry, and would couple to the Standard Model (SM) through kinetic mixing with the ordinary photon, $-\frac{1}{2}\epsilon F_{\mu\nu}A'^{\mu\nu}$, parametrized by the mixing strength $\epsilon \ll 1$, for a review see, e.g. [21]. A number of previous experiments, such as beam dump, fixed target,

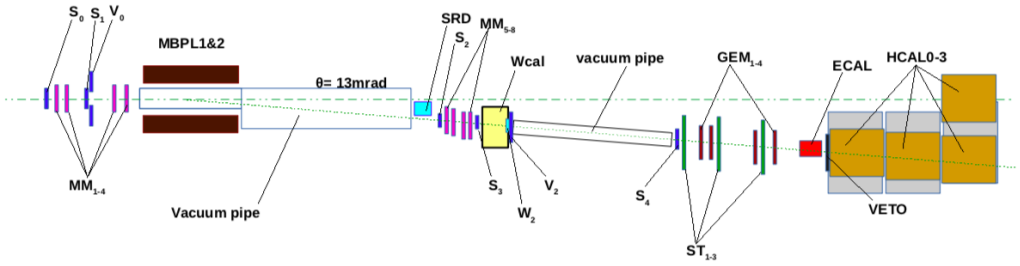

Figure 5. Schematic illustration of the setup to search for $A', X \to e^+e^-$ decays of the bremsstrahlung A', X produced in the reaction $eZ \to eZA'(X)$ of 100 GeV e^- incident on the active WCAL target.

collider and rare particle decay experiments have already put stringent constraints on the mass $m_{A'}$ and ϵ of such dark photons excluding, in particular, the parameter space region favored by the $g_\mu - 2$ anomaly, see e.g. [1]. However, a large range of mixing strengths $10^{-4} \lesssim \epsilon \lesssim 10^{-3}$ corresponding to a short-lived A' still remains unexplored. These values of ϵ could naturally be obtained from the loop effects of particles charged under both the dark and SM $U(1)$ interactions with a typical 1-loop value $\epsilon = ee_D/16\pi^2$, where e_D is the coupling constant of the $U(1)_D$ gauge interactions. The search for e^+e^- decays of new short-lived particles at the CERN SPS was performed by the NA64 experiment in 2017 [12]. Below we report the improved results from the NA64 experiment obtained using the data collected in 2018 in the new run at the CERN SPS performed after optimization of the experiment configuration and parameters.

4.1 The search method and the detector

The experiment employs the optimized electron beam from the H4 beam line in the North Area (NA) of the CERN SPS. The beam delivers $\simeq 5 \times 10^6$ e^- per SPS spill of 4.8 s produced by the primary 400 GeV proton beam with an intensity of a few 10^{12} protons on target. The NA64 setup designed for the searches of X bosons and A' is schematically shown in Fig. 5. Two scintillation counters, S1 and S2 were used for the beam definition, while the other two, S3 and S4, were used to detect the e^+e^- pairs. The detector is equipped with a magnetic spectrometer consisting of two MPBL magnets and a low material budget tracker. The tracker was a set of four upstream Micromegas (MM) chambers (T1, T2) for the incoming e^- angle selection and two sets of downstream MM, GEM stations and scintillator

hodoscopes (T3, T4) allowing the measurement of the outgoing tracks [5]. To enhance the electron identification the synchrotron radiation (SR) emitted by electrons was used for their efficient tagging and for additional suppression of the initial hadron contamination in the beam $\pi/e^- \simeq 10^{-2}$ down to the level $\simeq 10^{-6}$ [6, 11]. The use of SR detectors (SRD) is a key point for the hadron background suppression and improvement of the sensitivity compared to the previous electron beam dump searches. The dump is a compact electromagnetic (e-m) calorimeter WCAL made as short as possible to maximize the sensitivity to short lifetimes while keeping the leakage of particles at a small level. The WCAL was assembled from the tungsten and plastic scintillator plates with wave lengths shifting fiber read-out. The first few layers of the WCAL were read separately (preshower part). Immediately after WCAL there are veto counters W_2 and V_2, several meters downstream the signal counter S_4 and tracking detectors. These detectors are followed by another e-m calorimeter (ECAL), which is a matrix of 6×6 shashlik-type lead - plastic scintillator sandwich modules [11]. Downstream the ECAL the detector was equipped with a high-efficiency veto counter, and a thick hadron calorimeter (HCAL) [11] used as a hadron veto and muon identificator.

For the cuts selection, calculation of various efficiencies and background estimation the package for the detailed full simulation of the experiment based on Geant4 is developed. It contains the subpackage for the simulation of various types of Dark Matter particles based on the exact tree-level calculation of cross sections.

The method of the search for $A' \to e^+e^-$ decays is described in [7, 8]. The application of all further considerations to the case of the $X \to e^+e^-$ decay is straightforward. If the A' exists, it could be produced via the coupling to electrons wherein high-energy electrons scatter off a nuclei of the active WCAL dump target, followed by the decay into e^+e^- pairs:

$$e^- + Z \to e^- + Z + A'(X);\ A'(X) \to e^+e^- \tag{4.1}$$

The reaction (4.1) typically occurs within the first few radiation lengths (X_0) of the WCAL. The downstream part of the WCAL serves as a dump to absorb completely the e-m shower tail. The bremsstrahlung A' would penetrate the rest of the dump and the veto counter W_2 without interactions and decay in flight into an e^+e^- pair in the decay volume downstream the WCAL. A fraction (f) of the primary beam energy $E_1 = fE_0$ is deposited in the WCAL by the recoil electron from the reaction (4.1). The remaining part of the primary electron energy $E_2 = (1-f)E_0$ is transmitted through the dump by the A', and deposited in the second downstream calorimeter ECAL via the $A'(X) \to e^+e^-$ decay in flight, as shown in Fig. 5. The occurrence of $A' \to e^+e^-$ decays produced in e^-Z interactions would appear as an excess of events with two e-m-like showers in the detector: one shower in the WCAL and another one in the ECAL, with the total energy $E_{tot} = E_{WCAL} + E_{ECAL}$ equal to the beam energy (E_0), above those expected from the background sources.

4.2 Event selection and background evaluation

The candidate events were selected with the following criteria: (i) Small energy in the V_2: $E_{V_2} < 0.5MIP$ for 2017 data and $E_{W_2} < 0.9MIP$ for 2018 data (ii) The signal in the decay counter S4 is consistent with two MIPs; (iii) The sum of energies deposited in the WCAL+ECAL is equal to the beam energy within the boundaries determined by the energy resolution of these detectors. At least 25 GeV should be deposited in the ECAL; (iv) The shower in the WCAL should start to develop within a few first X_0, which is ensured by the preshower part energy cut; (v) The cell with maximal energy deposition in the ECAL should be (3,3); (vi) The lateral and longitudinal shape of the shower in the ECAL are consistent with a single e-m one. This requirement does not decrease the efficiency to signal events because the distance between e^- and e^+ in the ECAL is significantly smaller than the ECAL cell size. The rejection of events with hadrons in the final state was based on the veto $VETO$ and/or the energy deposited in the HCAL.

In order to increase the sensitivity to short-living X bosons (higher ϵ) the following optimization steps were performed before the 2018 run: (i) Beam energy increased to 150 GeV; (ii) Thinner counter W_2 was installed immediately after the last tungsten plate inside the WCAL box; (iii) more track detectors installed between WCAL and HCAL. In addition, the vacuum pipe was installed immediately after the WCAL, the distance between the WCAL and ECAL was increased. These changes would allow to perform the full track and vertex reconstruction for the events with the energy of the e^+e^- pair smaller than 80 GeV and perform immediate additional checks in case of signal observation. As in the prevoius analyses [11, 12], in order to check various efficiencies and the reliability of the MC simulations, we selected a clean sample of $\simeq 10^5$ $\mu^+\mu^-$ events with $E_{WCAL} < 0.6E_{beam}$ GeV originated from the QED dimuon production in the dump. This rare process is dominated by the reaction $e^-Z \to e^-Z\gamma; \gamma \to \mu^+\mu^-$ of a hard bremsstrahlung photon conversion into the dimuon pair on a dump nucleus. We performed various comparisons between these events and the corresponding MC simulated sample, and applied the estimated efficiency corrections to the MC events.

The main background in this search comes from the $K_S^0 \to \pi^0\pi^0$ events from K_0 mainly produced by hadrons misidentified as electrons [12]. We estimated this background using both simulation and data. For this, we selected the sample of neutral events changing the cut (ii) to $E_{S_4} < 0.5MIP$. This sample has 3 events in the 2017 data. No events were found with standard criteria in the 2018 data, for this reason we relaxed for this sample the shower shape cut. The distribution of neutral events is shown in Fig. 6. The MC sample of K_S^0 was simulated according to distributions predicted for the hadron interactions in WCAL. With this sample we calculated the number of neutral and signal-like events passing the criteria. This gives us the prediction of the number of background events: 0.06 for 2017 data and

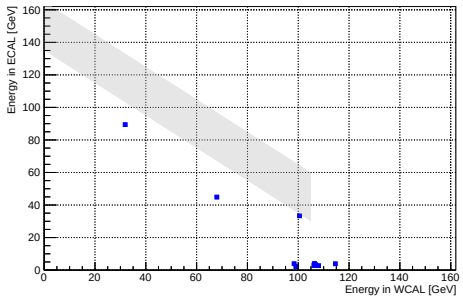

Figure 6. Distribution of selected e-m neutral events in the (E_{WCAL}, E_{ECAL}) plane from the 2018 data. Neutral events are shown as blue squares. The shadowed band represents the signal box region.

0.006 for the 2018 data. The smaller number of neutral events and lower background in the 2018 data are expected, because due to the higher distance between WCAL and ECAL less K_S^0 events pass the criteria (v) and (vi). In addition, the background is decreased because of the vacuum pipe before S_4.

The charge-exchange reaction $\pi^- p \to (\geq 1)\pi^0 + n + ...$ which can occur in the last layers of the WCAL with decay photons escaping the dump without interactions and accompanied by poorly detected secondaries is another source of fake signal. To evaluate this background we used the extrapolation of the charge-exchange cross sections, $\sigma \sim Z^{2/3}$, measured on different nuclei. The beam pion flux suppression by the SRD tagging is taken into account in the estimation. The contribution from the beam kaon decays in-flight $K^- \to e^- \nu \pi^+ \pi^- (K_{e4})$ and dimuon production in the dump $e^- Z \to e^- Z \mu^+ \mu^-$ with either $\pi^+\pi^-$ or $\mu^+\mu^-$ pairs misidentified as e-m event in the ECAL was found to be negligible.

Table 2. Expected numbers of background events in the signal box that passed the selection criteria (i)-(vi)

Source of background	2017 data	2018 data
punchthrough γ	< 0.001	< 0.0005
$K_S^0 \to 2\pi^0$	0.06 ± 0.034	0.005 ± 0.003
$\pi N \to (\geq 1)\pi^0 + n + ...$	0.01 ± 0.004	0.001 ± 0.0004
π^- hard brem. in the WCAL	< 0.0001	
$\pi, K \to e\nu$, K_{e4} decays	< 0.001	
$eZ \to eZ\mu^+\mu^-; \mu^\pm \to e^\pm \nu\nu$	< 0.001	
Total	0.07 ± 0.035	0.006 ± 0.003

Table 2 summarizes the estimated background inside the signal box. The main part of the total background uncertainty comes from the statistical error of the

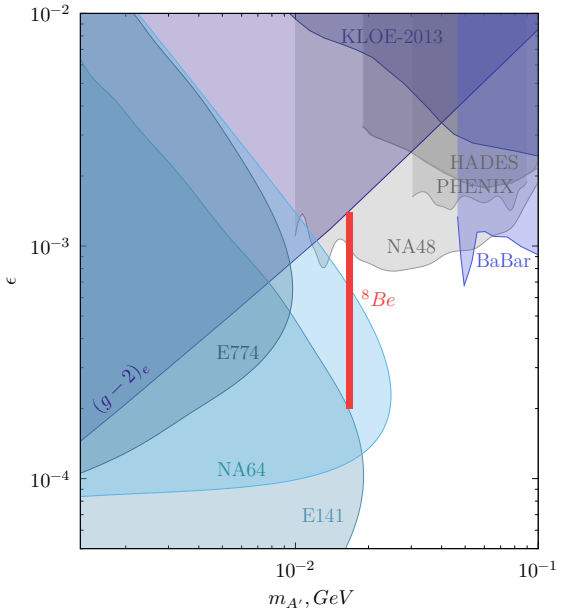

Figure 7. The preliminary 90% C.L. exclusion areas in the $(m_X; \epsilon)$ plane from the NA64 experiment (blue area). For the mass of 16.7 MeV, the $X - e^-$ coupling region excluded by NA64 is $1.2 \times 10^{-4} < \epsilon_e < 6.8 \times 10^{-4}$. The full allowed range of ϵ_e explaining the ^{8}Be* anomaly, $2.0 \times 10^{-4} \lesssim \epsilon_e \lesssim 1.4 \times 10^{-3}$ [19, 20], is also shown (red area). The constraints on the mixing ϵ from the experiments E774, E141, BaBar, KLOE, HADES, PHENIX, NA48, and bounds from the electron anomalous magnetic moment $(g-2)_e$ [29] are also shown, see Ref.[21].

number of observed e-m neutral events. There is also the uncertainty from the cross sections of the π, K charge-exchange reactions on heavy nucleai (30%).

After determining and optimizing the selection criteria and estimating the background levels, we examined the signal box and found no candidates.

4.3 Preliminary results on the $X \to e^+e^-$ and $A' \to e^+e^-$ decays

The combined 90% confidence level (C.L.) upper limits for the mixing strength ϵ were determined from the 90% C.L. upper limit for the expected number of signal events, $N_{A'}^{90\%}$ by using the modified frequentist approach for confidence levels (C.L.), taking the profile likelihood as a test statistic in the asymptotic approximation [24–26]. The total number of expected signal events in the signal box was the sum of expected events from the 2017 and 2018 runs:

$$N_{A'} = \sum_{i=1}^{2} N_{A'}^i = \sum_{i=1}^{2} n_{EOT}^i \epsilon_{tot}^i n_{A'}^i(\epsilon, m_{A'}) \tag{4.2}$$

where ϵ_{tot}^i is the signal efficiency in the run i, and $n_{A'}^i(\epsilon, m_{A'})$ is the number of the $A' \to e^+e^-$ decays in the decay volume with energy $E_{A'} > 25$ GeV per EOT,

calculated under assumption that this decay mode is predominant, see e.g. Eq.(3.7) in Ref. [8]. Each i-th entry in this sum was calculated by simulating signal events for the corresponding beam running conditions and processing them through the reconstruction program with the same selection criteria and efficiency corrections as for the data sample from the run-i. In the overall signal efficiency for each run the acceptance loss due to pileup in the veto detectors was taken into account. The total effective number of collected $n_{EOT} = 8.4 \times 10^{10}$ EOT takes into account the trigger suppression factor and the data acquisition system (DAQ) dead time. The trigger (SRD tagging) efficiency were obtained using unbiased samples of events that bypass selection criteria and were found to be 0.95 (0.97) with a small uncertainty 2%. The A' yield from the dump was calculated as described in Ref.[9]. These calculations were cross-checked with the calculations of Ref.[27, 28]. The $\lesssim 10\%$ difference between the two calculations, presumably due to the difference in computation program used, was accounted for as a systematic uncertainty in $n_{A'}(\epsilon, m_{A'})$. The total systematic uncertainty on $N_{A'}$ calculated by adding all errors in quadrature did not exeed $\simeq 25\%$ for both runs. The preliminary combined 90% C.L. exclusion limits on the mixing ϵ as a function of the A' mass is shown in Fig. 7 together with the current constraints from other experiments. Our preliminary results exclude X-boson as an explanation for the ^{8}Be* anomaly for the $X - e^-$ coupling $\epsilon_e \lesssim 6.8 \times 10^{-4}$ and mass value of 16.7 MeV, leaving the still unexplored region $6.8 \times 10^{-4} \lesssim \epsilon_e \lesssim 1.4 \times 10^{-3}$ as quite an exciting prospect for further searches. However, more work has to be done for better understanding of the signal efficiency loss in this search, in particular due to the e-m signal shower energy leak to the W_2 counter.

5 Study of dimuon production by using tracker

Dimuon events originate from the QED production, dominated by the the muon pair photoproduction by a hard bremsstrahlung photon conversion on a target nucleus:

$$e^- Z \to e^- Z\gamma; \gamma Z \to \mu^+\mu^- Z. \tag{5.1}$$

with some contribution from $\gamma\gamma \to \mu^+\mu^-$ fusion process. The $\mu^+\mu^-$ pairs were characterised by the HCAL energy deposition of $\simeq 10$ GeV. This rare process whose fraction of events with $E_{ECAL} \lesssim$90 GeV was $\lesssim 10^{-5}$/EOT served as a benchmark allowing to verify the tracker performance and as a reference for the background prediction.

5.1 Simulation of $\gamma + Z \to \mu^+\mu^- Z$ in 2018 visible mode setup

The data from a selected dimuon sample are compared to a detailed MC simulation. The simulation was performed using 150 GeV electrons as primaries and by biasing the cross section with a factor 200 for the interaction $\gamma + Z \to \mu^+\mu^- Z$. The $\sim 8 \cdot 10^5$

events containing a dimuon production are then used for the comparison with the data. To avoid a biased sample all the cuts used for the selection in the data are applied to the simulation as well without assuming any prior knowledge over the nature of the event. These cuts will be reviewed in Sec.5.2.

A realistic beam profile was extracted from the electron calibration. The sample was further purified by requiring recorded energy between 5 MeV and 100 MeV for both SRD counters. The beam profile was then recovered by fitting the XY position recorded by the two upstream Micromegas with a 2D Gaussian. The two fits agree within 100 μm precision for both $\sigma_X \approx 4.13$ mm and $\sigma_y \approx 1.40$ mm. Fig.8 shows a comparison of the reconstructed hit-position after all these corrections were applied to the simulation in the GEM module 4 using a dimuon sample extracted from the data. All other modules show a similar behaviour. To improve the agreement between data and Monte Carlo several strategies were used. Both the resolution of the detectors and the maximum possible separation between two hits were added to the simulation after a detail studies of the GEM output. And the same reconstruction chain was used to ensure no bias in the hit or tracks selection.

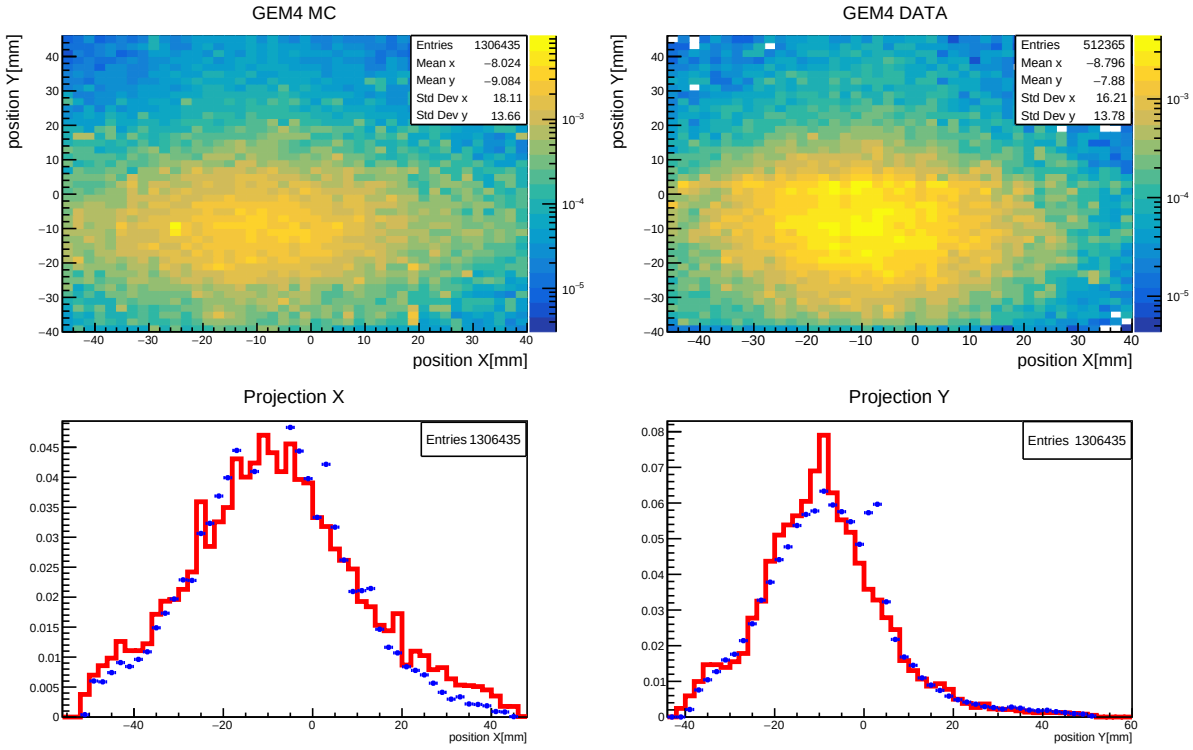

Figure 8. Hit position recorded in last GEM before ECAL for MC simulated (Red curve) and data (Blue dots) $\gamma + Z \to \mu^+\mu^- Z$ events

5.2 $\gamma + Z \to \mu^+\mu^- Z$ events recorded in 2018 visible mode setup

A dimuon sample was selected using all events collected during the visible mode of 2018. The beam quality was improved by requiring zero energy deposited in the Catcher placed off-beam upstream the WCAL and a reconstructed momentum in the range between 140 and 160 GeV . This was done to ensure a well-defined energy distribution not biased by the physical trigger employed in the experiment. A cut of 2 GeV $<E_{hcal} <$ 6.35 GeV for the first two HCAL modules placed after the ECAL and energy of less than 90 GeV in the WCAL selects dimuons events. The cuts on the HCAL modules is used to select a clean sample of dimuons leaving a double-MIP signature, where the third HCAL module is excluded to increase the acceptance and the additional cut on the WCAL is used to further suppress contribution coming from the region affected by the physical trigger. Finally, an energy deposited of at least 1 MIP is required in the scintillator downstream the WCAL (S4), while at least 1.8 MIP is requested in the Veto behind the ECAL. This last cuts is used not only to increase the purity of dimuon in the sample, but also to select a sample with kinematics closer to the one expected from an hypothetical dark matter candidate. This makes the comparison with the Monte Carlo more significant for our search.

Although these cuts are expected to select mainly dimuon coming from γ produced in the em-shower generated by the 150 GeV electron in the beam, a contribution is also expected from the hadron contamination in the beam. The physical trigger employed in the experiment further increases such contribution, as the requirement of low energy deposit in the WCAL bias the beam composition to particles with high penetration power. To solve this issue a cut on the SRD detector and the pre-shower of WCAL is used. These cuts were used in the past for NA64 analysis and are expected to reject hadrons and muons at a level $< 10^{-5}$. To cross-check that the contamination is correctly removed, an independent method based on the beam profile is used. The beam profile significantly differs between electrons and hadrons as the H4 beamline is tuned for electrons. Both profiles are recovered from the data using a calibration run of electron/hadron respectively. The ratio between the two is estimated by mixing the two templates obtained from the calibration runs until the best agreement with the measured beam profile is reached using a χ^2-test. The result is summarized in Fig.9, where the beam profile of events selected with the dimuon-selection cuts discussed above are compared before and after the SRD criteria is applied. Before the SRD cut, the fits predict a contamination of roughly 50% of hadron in the sample. After the cuts, the beam profile converges to the templates obtained in the calibration run, with the fit returning a value of contamination compatible with zero.

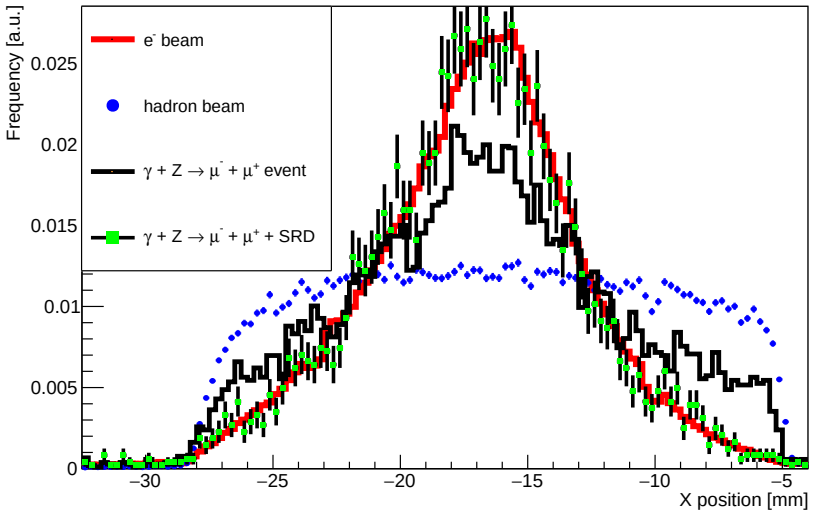

Figure 9. Beam profile recorded by MM1(first Micromegas module upsteram) for hadron calibration run (blue dots), electron calibration run (red line), events selected with dimuons cuts from data collected with the physical trigger (black line) and those same events after SRD cut is applied (green square). Fits using the templates obtained from the calibration run show a level of contamination of ∼50% in the dimuon sample.

5.3 Comparison

To show that there are no significant differences in the tracking procedure between simulation and data the reconstructed angle and the energy deposited in the WCAL were used as figure of merit. As the interaction $\gamma + Z \rightarrow \mu^+\mu^- Z$ will have their vertex inside the WCAL, only vertex compatible with this assumption are selected for the comparison. In practice, a vertex is accepted if its position lies within 3σ of the expected WCAL position, where σ was fitted using a Gaussian from the distribution of pure dimuon pair selected from the simulation. After all such cuts are applied, the angle of the surviving vertex candidates is compared between simulation and data. Fig.10 shows the correlation between energy deposited and angle reconstructed for all vertex candidates selected. The energy deposition for data and simulation are in excellent agreement after all selection criteria are applied. The comparison with the angle is also reasonable, with the peak of the angle distribution being 2.9 mrad for simulation and 2.7 mrad for data with the two distribution matching to a good degree. It can be seen that a larger tail in the reconstructed angle is observed in the simulation. By integrating the number of events from 0 to 10 mrad one can quantify this difference to ∼6%. As the typical dark matter scenario predicts an angle <2mrad this is not expected to affect our search.

The dimuon sample is also used to estimate the inefficiency of the tracking pro-

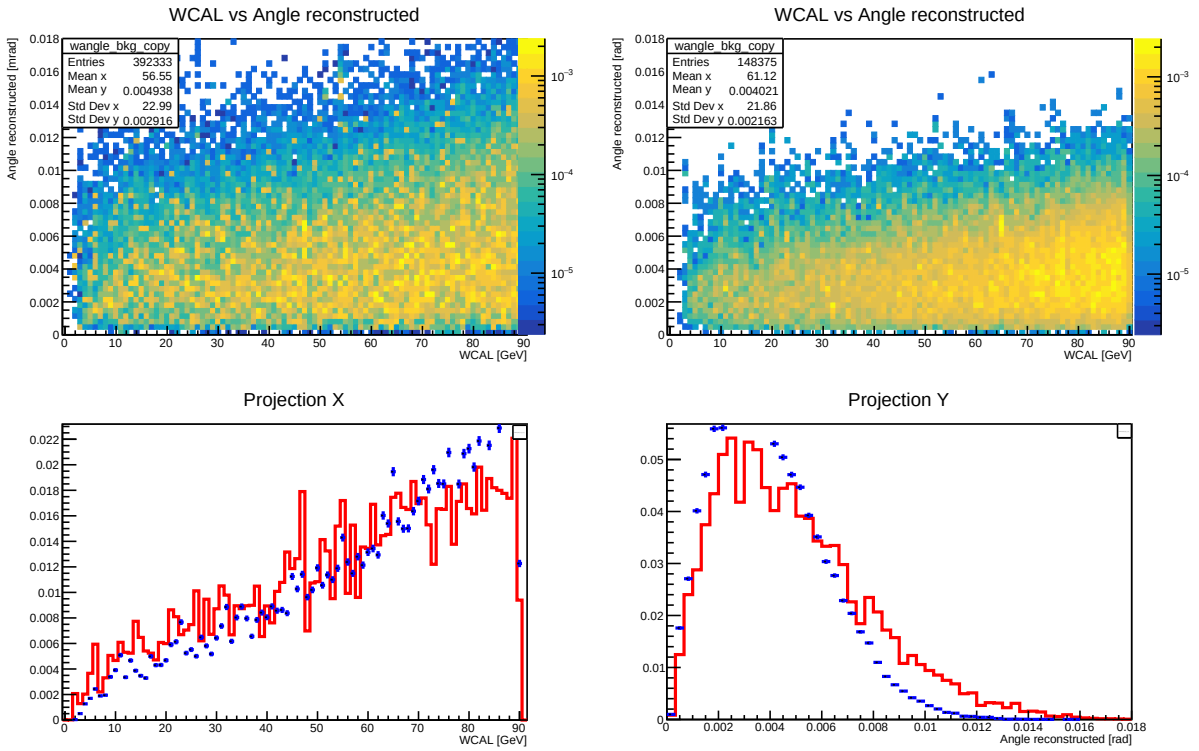

Figure 10. Top: Energy deposited in the WCAL vs reconstructed angle of all vertex within 3σ from the WCAL position for simulated $\gamma + Z \to \mu^+\mu^- Z$ (left) and a sample of data from 2018 visible mode run with selection criteria for dimuon (right). The two bottom plots show the comparison of the two projection for the two groups. Data are drawn with blue dots, simulation is plotted through a red line.

cedure in order to correctly estimate the signal yield. The reason for this differences are the inefficiencies of the GEM modules, fail of clusterization in some events or differences in the efficiency of the tracking procedure due to the simplifications used in the MC. The cuts applied to the sample are divided into four steps: i) at least two hits per GEM are required in the decay volume as a minimal condition for tracking. ii) events with a GEM module recording more than 5 hits are rejected as well from the analysis as incompatible with a single $\gamma + Z \to \mu^+\mu^- Z$ vertex in the decay volume. The MC predicts 68% of $\gamma + Z \to \mu^+\mu^- Z$ to be within the GEM acceptance of the 2018 setup. This low acceptance is explained from the fact that the GEMs position is optimized to resolve very close two hits track coming from the decay of X and is therefore less efficient for dimuon searches. These first two cuts do not depend on the track-fitting procedure but instead on the clusterization performed by CORAL [33] and the efficiency of the GEMs modules, which are not present in the simulation. A factor of 0.8 is used to account for this as result of the comparison between data and Monte Carlo. iii) the tracking procedure is applied to the events that survived the

cut	efficiency MC	efficiency Data	MC / DATA
Hits			
hits per GEM ≥ 2	0.68 ± 0.01	0.58 ± 0.01	0.85
hits per GEM ≤ 5	0.68 ± 0.01	0.55 ± 0.01	0.80
tracking			
Vertex distance ≤ 3 mm	0.63 ± 0.01	0.49 ± 0.01	0.77
Vertex in decay volume	0.62 ± 0.01	0.48 ± 0.01	**0.77**

Table 3. efficiency of cuts based on tracking criteria for a clean sample of simulated $\gamma + Z \to \mu^+\mu^- Z$ and dimuon selected from the data for 2018. Hits cuts report efficiencies on cuts based exclusively on information coming from the single GEM modules. Tracking cuts are reporting efficiency after the tracking procedure is applied.

two first requirements, only events with at least one vertex with minimal distance between tracks lower than 3 mm are selected. iv) the last cut requires the vertex position to be compatible with a vertex inside the decay volume, using the same cuts described above. The number of events surviving the requirement of at least one vertex in the decay volume was found to be slightly smaller in the data, notably the disagreement between the ratio of good vertex reconstructed inside the decay volume is <1%. Accounting the smaller efficiency in the vertex-reconstruction in the data on the top of what was estimated for the hits reconstruction, a total factor of 0.77 less efficiency is estimated in the data within respect to the Monte Carlo. This factor is used for the correction of estimated signal yield in 2018 for the analysis involving tracking procedures. A summary of the efficiency can be found in Table 3.

5.4 Analysis of 2018 collected data using tracker

One of the main limitations of previous analysis in the context of NA64 visible mode setup was a strict cut on the Veto behind the WCAL reducing the efficiency for low energy X produced during the late stages of the em-shower. Although one would expect from a first order approach most of X to be produced at high energy at the beginning of the shower, a large fraction of X bosons with energies between 30 and 50 GeV is expected because of the high multiplicity of the shower at later stages. These X are rejected in an analysis based exclusively on the requirement of low energy deposited in the Veto at the end of the dump. There are two main reasons for this: short-lived particle have a high chance of decaying before the end of the dump if the decay length is not boosted significantly, hence they have a higher chance of being rejected by the Veto. Secondly, when X is produced at the late stages of the shower, the chance for the remaining particles in the dump to leave a large signal in the Veto is high. On the other hand, if X is produced at the beginning of the WCAL most of the energy of the shower is lost and the remaining e^- does not have enough momentum to reach the last layer of the WCAL and thus the event passes

the selection.

The disadvantage of this analysis is overcome using the tracker instead: the presence of a vertex with a small angle in the decay volume substitute the criteria of no energy in the WCAL and X is able to pass the selection criteria even if its energy is low. On the other hand, the analysis has shortcomings for dark matter produced with high boost: very high energetic dark matter will have a very small aperture angle that is often not resolvable by the GEM modules. Fig. 11 summarizes this claim

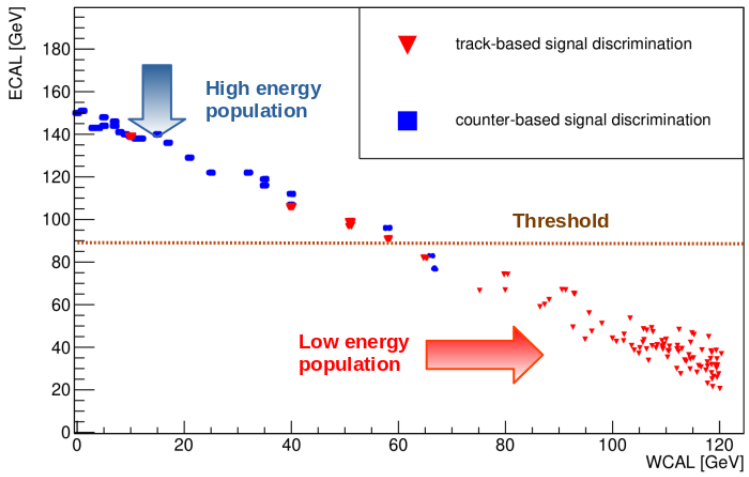

Figure 11. Simulated events with Xproduction inside the WCAL in 2018 visible mode setup. Events passing selection criteria based on tracking are plotted in red, while events surviving selection criteria based on Veto and S4 cut are plotted with blue square. Estimated optimal threshold to switch between selection criteria is shown with a brown line.

by comparing a sample of simulated X using these two different selection criteria. The plot shows that two population of X exist in a beam dump experiment and they can be distinguished using the energy deposited in the ECAL downstream the dump. Due to their different kinematics, it is convenient to treat the two population separately and apply different final selection criteria. An analysis that combines the two approaches is structured as follows: first standard cuts are used to purify the sample from a large number of hadrons selected by the physical trigger. These cuts are the same employed in previous searches as they are independent of the exact signal scenario. After that, a signal region is defined by asking energy in the WCAL smaller than 105 GeV , and total energy deposited between WCAL and ECAL to be equal to the nominal beam energy with an uncertainty estimated at 10%. Finally, one looks at the energy recorded in ECAL to decide the best selection criteria to define if the event is compatible with the production of dark matter. If $E_{ECAL} \geq E_{thr}$ one uses no energy deposited in the Veto and a signal larger than 0.8 MIP in S4 as the final requirement, else the final selection criteria will be the presence of a vertex in the

M_X [GeV]	ϵ	N_X (counter analysis)	N_X (counter+tracking analysis)
0.0167	0.000316	1.50	1.85
0.0167	0.0006	1.25	1.28
0.0167	0.0001	0.23	0.28
0.0167	0.0007	0.78	0.78
0.005	0.004	2.11	2.11
0.0167	0.00018	0.85	1.02
0.022	0.000316	0.65	0.79

Table 4. N_X expected for 10^{10} EOT for different signal scenarios. Different types of analysis are compared: the counter analysis uses only the veto behind Tungsten ECAL for the final discrimination. Counter + tracking uses instead cuts based on GEMs as described in Sec.5.3 depending on the energy detected by the downstream ECAL using $E_{thr} = 75$ GeV as threshold.

decay volume with a reconstructed angle smaller than 3 mrad . Table 4 compares the expected number of X for 10^{10} EOTS using the counter-based approach compared to the new one for different X couplings. Although for some scenario the boost can be significant, for X with very small decay time the weight of such low energetic X is so small that the two approaches ultimately reach very close results. The background for this searches could arise from particles punching through the WCAL and leaving a signature in the trackers downstream. Such contribution could arise either from large energy γ punching through the WCAL and converting in the last few layers or by hadrons interacting in the dump. No background was found in MC simulations as large as 10^7 EOT. To estimate the background for a larger number of EOTS, K^0_S was used as benchmark process, as its pure-electromagnetic decay channels and short decay length are expected to be compatible with the one of the signal. A dedicated simulation was performed to estimate the contribution of such interaction for the statistic accumulated in 2018. The energy spectrum of K^0_S was approximated using an exponential distribution fitted using a dedicated MC with an energy cut-off of 18 GeV, as K^0_S with lower momentum would not be able to leave enough energy in the ECAL to enter in the signal region. By applying tracking-criteria over this sample it was estimated that a rejection of 10^{-3} can be conservatively achieved for this background, mainly through a cut on the reconstructed angle with some small correction due to the lower acceptance of the setup. As no neutral events were found using the standard criteria of $E_{S4} < 0.5MIP$ in 2018 data, it was estimated a number of background event of 0.006 for the counter analysis, see Sect. 4. By adding the additional suppression coming from the angle using the trackers, one can conservatively estimate the background contribution from K_S to be at a level of < 0.001.

Table 5 summarizes the source of background expected for the combined counter

background source	estimated background
γ punchtrough from em-shower	<0.01
π^- punchtrough	<0.001
$K_S^0 \to \pi^- + \pi^+$	<0.001
$K_S^0 \to \pi^0 + \pi^0$,$\pi^0 \to \gamma + e^- + e^+$	<0.001

Table 5. background sources for NA64 visible mode tracking analysis

and tracking analysis. The conclusion is that the background should be under control for the full dataset accumulated during 2018 visible mode.

The analysis defined on the selection criteria described above was tested on the full data sample collected during 2018, amounting to $n_{eots} \approx 3 \times 10^{10}$. No events were found passing all the selection criteria chosen for the analysis. Three events were observed with energy very close to the minimal allowed by the cut $E_{WCAL} < 105$ GeV (energy between 25 GeV and 40 GeV approximately) compatible with the presence of two particles in the decay volume. However, no reliable vertex could be reconstructed from such events, leading to the conclusion that those events were caused by a small leak from the WCAL with no physical vertex. This result is compatible with the one obtained by the counter analysis, and shows the complementarity of the two approaches.

6 Detector upgrades for the 2021 run

Several detector issues must be addressed for NA64 to collect data as efficiently as possible in the 2021 run. The upgrades proposed are designed to improve the reliability of the detector and the trigger/DAQ livetime. The improvement in data-taking efficiency will come mainly from the replacement of DAQ components partly described previously. Several modifications to the trigger and front-end readout are required to achieve the live-time improvement. The combined improvement will reduce the experiment's overall deadtime (i.e., total beam time for which the experiment is not live) by 10%, equivalent to adding potentially 0.5 weeks to a 5 week run. To increase the overall signal efficiency and improve background rejection the following upgrade of the setup is planned:

(i) additional number of the MM, GEM, ST stations are planned to be installed. A possible use of Si pixels as the tracker for the $X \to e^+e^-$ decay search might also be considered.

(ii) two fast beam hodoscopes in the upstream part of the setup

(iii) higher transversely segmented SRD detector with improved readout

(iv) large Veto HCAL (VHCAL) in front of the ECAL to reject large angle neutral secondaries from the upstream e^- hadronic interactions

(v) further improvement of the DAQ and the analysis program are foreseen to ensure a substantial data collection of $n_{eot} \simeq 10^{12}$ events in 2021.

As mentioned above, in order to probe the theoretically interesting parameter space $\epsilon \simeq 10^{-5} - 10^{-3}$ and $m_{A'} \lesssim 1$ GeV the number of accumulated electrons on target is required to be around $n_{eot} \gtrsim 5 \times 10^{12}$ or more, and a very low background rate. Assuming the beam rate $\simeq 10^7$ e^-/spill and $\simeq$4000 good spills/day, about 6 months of data taken are required. Therefore, in order to use more effectively the H4 line, current a new area at H4 for the permanent NA64 detector location is currently under preparation to avoid loss of the beam time for the detector assembly, installation and commissioning. The NA64 team also participate in this work.

7 Summary

In the 2018 run the NA64 detector was fully operational and working. Good quality data of $\simeq 2 \times 10^{11}$ EOT were collected in total. Although NA64's runs were quite successful and produce significant physics results, we believe we have only begun to exploit the physics potential of the proposed experimental technique and detector. The further runs will provide us with the opportunity to continue this program to meet our original goals for the proposal.

(i) The analysis of the combined data sample from 2016-2018 runs on the A' invisible decay mode is completed. A search for sub-GeV dark matter production mediated by the vector boson A', called dark photon, is performed by the NA64 experiment in missing energy events from 100 GeV electron interactions in an active beam dump at the H4 beam. From the analysis of the data collected in the years 2016, 2017, and 2018 with 2.84×10^{11} electrons on target no evidence of such a process has been found. The most stringent constraints on the A' mixing strength with photons and the parameter space for the scalar and fermionic dark matter in the mass range $\lesssim 1$ GeV are derived. Thus, demonstrating the power and advantage of the NA64 active beam dump approach for the dark matter search. The results have been published as CERN preprint CERN-EP-19-166 and are further submitted to arXiv and Phys. Rev. Lett.

(ii) The preliminary results on a direct search for a new 16.7 MeV boson (X) which could explain the anomalous excess of e^+e^- pairs observed in the excited ^{8}Be* nucleus decays are obtained. The data were collected in two runs, in 2017 and 2018. With total statistics corresponding to 8.4×10^{10} electrons on target no evidence for such decays was found, allowing to set preliminary limits on the

$X - e^-$ coupling in the range $1 \times 10^{-4} \lesssim \epsilon_e \lesssim 6 \times 10^{-4}$ excluding part of the allowed parameter space. We also set new preliminary bounds on the mixing strength of photons with dark photons (A') from non-observation of the decay $A' \to e^+e^-$ of the bremsstrahlung A' with a mass $\lesssim 24$ MeV. However, more work has still to be done for better understanding of the signal efficiency loss in this search, in particular due to the e-m signal shower energy leak to the W_2 counter.

(iii) Lessons from the 2018 run
- The detector worked well at the intensity up to $\simeq 10^7$ e^-/ spill.
- Assuming such intensity and on average $\simeq 4000$ good spill per day means that accumulation of up to $\gtrsim 5 \times 10^{12}$ EOT during 6 months of running after LS2 is feasible.
- The results obtained with such number of EOT will allow us to probe full parameter space for scalar and Majorana sub-GeV dark matter models.

(iv) The 2021 runs
- preparation of the new NA64 area at H4 is in progress,
- $\gtrsim 5 \cdot 10^{10}$ EOT are expected to be collected for visible mode at 150 GeV,
- Plan for the 2021 runs is to accumulate in total $\simeq 10^{12}$ EOT in order to cover yet unexplored areas in the sub-GeV Dark Matter parameter space and to perform a more sensitive search for the $A'(X) \to e^+e^-$ decays.

The analysis of the data sample collected before LS2 in 2016-2018 and the preliminary results obtained provide a significant contribution to the update of the European Strategy for Particle Physics and can also play an essential role in helping to plan for a future dark sector experiments at the SPS.

8 Publications

Since the last NA64 SPSC report in June 2018 the collaboration has completed the physics analyses of the 2016-2018 data sample on the search for the $A' \to$ *invisible* decay and analysis of the 2017-2018 data on the search for the $X \to e^+e^-$ of the 17 MeV X-boson from the ^{8}Be anomaly and the $A' \to e^+e^-$ decays of dark photons, which are planned to be submitted for publication:

(i) NA64 collaboration: D. Banerjee et al. "Dark matter search in missing energy events with NA64", CERN-EP-2019-166, arXiv:1906.00176, to be submitted to PRL.

(ii) NA64 collaboration: D. Banerjee et al. "Improved limits on a new X(16.7) boson and dark photons decaying into e^+e^- pairs with NA64". Paper in preparation for publication.

The collaboration is contributing to several International Conferences and topical Workshops where NA64 recently published or preliminary physics results from combined 2016-2018 data analyses were presented. In the past year (June 2018 to June 2019), the NA64 speakers presented 8 talks to Physics Conferences. More contributions are already foreseen in future 2019 Conferences.

References

[1] M. Battaglieri *et al.*, arXiv:1707.04591 [hep-ph].

[2] J. Beacham *et al.*, (2019). arXiv:1901.09966 [hep-ex].

[3] R. Alemany *et al.*, arXiv:1902.00260 [hep-ex].

[4] C. Patrignani *et al.* [Particle Data Group], Chin. Phys. C **40**, 100001 (2016).

[5] D. Banerjee, P. Crivelli and A. Rubbia, Adv. High Energy Phys. **2015**, 105730 (2015).

[6] E. Depero *et al.*, Nucl. Instrum. Meth. A **866**, 196 (2017).

[7] S. N. Gninenko, Phys. Rev. D **89**, 075008 (2014).

[8] S. Andreas *et al.*, arXiv:1312.3309 [hep-ex].

[9] S. N. Gninenko, N. V. Krasnikov, M. M. Kirsanov and D. V. Kirpichnikov, Phys. Rev. D **94**, 095025 (2016).

[10] S. N. Gninenko, D. V. Kirpichnikov, M. M. Kirsanov and N. V. Krasnikov, Phys. Lett. B **782**, 406 (2018).

[11] D. Banerjee *et al.* [NA64 Collaboration], Phys. Rev. D **97**, 072002 (2018).

[12] D. Banerjee *et al.* [NA64 Collaboration], Phys. Rev. Lett. **118**, 011802 (2017).

[13] J. P. Lees *et al.* [BaBar Collaboration], arXiv:1702.03327 [hep-ex].

[14] E. Cortina Gil *et al.*, [NA62 Collaboration], arXiv:1903.08767 [hep-ex].

[15] A. A. Aguilar-Arevalo *et al.* [MiniBooNE Collaboration], Phys. Rev. D **98**, 112004 (2018) .

[16] I. Antcheva *et al.*, Comput. Phys. Commun. **180**, 2499 (2009).

[17] E. Gross, "LHC statistics for pedestrians," CERN-2008-001, p.71, CERN, 2008.

[18] A. Krasznahorkay et al., Phys. Rev. Lett. **116**, 042501 (2016).

[19] J. Feng J. L. Feng, B. Fornal, I. Galon, S. Gardner, J. Smolinsky, T. M. P. Tait, Ph. Tanedo, Phys. Rev. Lett. **117**, 071803 (2016).

[20] J. L. Feng, B. Fornal, I. Galon, S. Gardner, J. Smolinsky, T. M. P. Tait, Ph. Tanedo, Phys. Rev. D **95**, 035017 (2017).

[21] M. Battaglieri et al.., US Cosmic Visions: New Ideas in Dark Matter 2017: Community Report, arXiv:1707.04591.

[22] E. Nardi, C. D.R. Carvajal, A. Ghoshal, D. Meloni, M. Raggi, arXiv:1802.04756.

[23] J. Kozaczuk, Phys. Rev. D **97**, 015014 (2018).

[24] T. Junk, Nucl. Instrum. Meth. A **434**, 435 (1999).

[25] G. Cowan, K. Cranmer, E. Gross, O. Vitells, Eur. Phys. J. C **71**, 1554 (2011).

[26] A. L. Read, J. Phys. G **28**, 2693 (2002).

[27] Analysis of 2018 collected data using trackers Y. S. Liu, D. McKeen and G. A. Miller, Phys. Rev. D **95**, 036010 (2017)

[28] Y. S. Liu and G. A. Miller, Phys. Rev. D **96**, 016004 (2017).

[29] H. Davoudiasl, H. S. Lee, and W. J. Marciano, Phys. Rev. D **89**, 095006 (2014).

[30] http://pdg.lbl.gov/

[31] https://github.com/GenFit/GenFit

[32] S.N. Gninenko, N.V. Krasnikov, M.M. Kirsanov, D.V. Kirpichnikov, Missing energy signature from invisible decays of dark photons at the CERN SPS, Phys. Rev. D 94, 095025 (2016), arXiV:1604.08432 [hep-ph]

[33] P. Abbon *et al.* [COMPASS Collaboration], Nucl. Instrum. Meth. A **577** (2007) 455 doi:10.1016/j.nima.2007.03.026 [hep-ex/0703049].